Letter

Pole analysis on the doubly charmed meson in $D^0D^0\pi^+$ mass spectrum

Ling-Yun Dai,[1,2,*] Xiang Sun,[1,2] Xian-Wei Kang,[3,4] A. P. Szczepaniak,[5,6,7,†] and Jie-Sheng Yu[1,2,‡]

[1]*School of Physics and Electronics, Hunan University, Changsha 410082, China*
[2]*Hunan Provincial Key Laboratory of High-Energy Scale Physics and Applications, Hunan University, Changsha 410082, China*
[3]*Key Laboratory of Beam Technology of the Ministry of Education, College of Nuclear Science and Technology, Beijing Normal University, Beijing 100875, China*
[4]*Beijing Radiation Center, Beijing 100875, China*
[5]*Physics Department, Indiana University, Bloomington, Indiana 47405, USA*
[6]*Center for Exploration of Energy and Matter, Indiana University, Bloomington, Indiana 47403, USA*
[7]*Thomas Jefferson National Accelerator Facility, Newport News, Virginia 23606, USA*

(Received 15 August 2021; accepted 1 March 2022; published 23 March 2022)

In this paper, we study the scattering amplitudes of $D^0D^0\pi^+$-$D^{*+}D^0$ coupled channels based on the K matrix within the Chew-Mandelstam formalism. The $D^0D^0\pi^+$ invariant mass spectrum of LHCb is fitted, and the pole parameters of the T_{cc}^+ are extracted. The analysis of pole behavior suggests that the T_{cc}^+ may originate from a $D^{*+}D^0$ virtual state and is formed as a result of an interplay between an attractive interaction between D^0 and D^{*+} and coupling to $D^0D^0\pi^+$ channel.

DOI: 10.1103/PhysRevD.105.L051507

I. INTRODUCTION

For over half a century, the quark model served as the fundamental template for constructing hadrons [1,2]. Dozens of known hadrons can be classified according to this model with three quarks in a baryon and a quark-antiquark pair in a meson. However, the requirement of color neutrality alone does not preclude existence of more complicated structures, including, for example, tetraquarks and pentaquarks. In the last 20 yr, several candidates for such multiquark hadrons, specifically containing heavy quarks, have been observed by the Belle, *BABAR*, BESIII, D0, CDF, CMS, and LHCb experiments [3–13]. A significant number of these states are found lying close to various thresholds for decays into nonexotic hadrons. For example, the $X(3872)$ discovered by Belle [3] is in a mass region that is not expected to host a quark-model-like charmonium state, but it is only ∼1 MeV away from the $D\bar{D}^*$ threshold. The proximity to this threshold makes it likely to be a $D\bar{D}^*$ molecule [14–16]. Recently, the LHCb Collaboration announced observation of another X-like candidate, this time, however, containing two charm quarks instead of a charm-anticharm pair labeled T_{cc}^+ [17,18]. The T_{cc}^+ was observed, with a 21.7σ significance in the $D^0D^0\pi^+$ invariant mass spectrum near threshold, i.e., with the mass close to the $X(3872)$, $M_{T_{cc}^+} - (M_{D^{*+}} + M_{D^0}) = -237 \pm 61\ \mathrm{keV/c^2}$, and width $\Gamma_{T_{cc}^+} = 410 \pm 165$ keV. Because two charm quarks alone cannot form a color singlet hadron, if confirmed, the T_{cc}^+ would be clear evidence of a multiquark hadron. The small width indicates that there could be a pole in the relevant partial wave close to the D^0D^{*+} threshold, However, since D^* decays to $D\pi$, rescattering between $D^0D^0\pi^+$ and D^0D^{*+} should be taken into account in determining the pole parameters [19–24].

There have been some theoretical studies of the T_{cc}^+; see, e.g., [25–30]. In this paper, we use effective range approximation and consider the coupled amplitudes for production of $D^0D^0\pi^+$ and $D^{*+}D^0$ final states. By fitting to the line shape, we obtain a solution for the production amplitude which enables analytical continuation to the complex energy plane where we extract the pole parameters. Finally, by analyzing the pole position we speculate on the possible nature of the T_{cc}^+ peak.

II. FORMALISM

We need analytical amplitudes to describe the $D^0D^0\pi^+$ invariant mass spectrum in order to obtain accurate pole information. The T_{cc}^+ is found in the $D^0D^0\pi^+$ invariant mass spectrum near the $D^{*+}D^0$ threshold of 3875.09 MeV. One also notices that the branching ratio of $D^{*+} \to D^0\pi^+$ is $67.7 \pm 0.5\%$ [31]. The D^* and $D\pi$ are physically two

*dailingyun@hnu.edu.cn
†aszczepa@indiana.edu
‡yujiesheng@hnu.edu.cn

Published by the American Physical Society under the terms of the Creative Commons Attribution 4.0 International license. Further distribution of this work must maintain attribution to the author(s) and the published article's title, journal citation, and DOI. Funded by SCOAP³.

different states. The former is a resonance (presumably a $q\bar{q}$ bound state in quenched QCD), and the latter is in a two-hadron continuum. The two are distinguished, for example, by the value of the corresponding thresholds, which is relevant given the proximity of the T_{cc} to the $DD\pi$ threshold. Hence, it is natural to consider the $D^0D^0\pi^+$-D^0D^{*+} coupled channels. The analytical coupled channel amplitudes near threshold can be parametrized using a real, symmetric 2×2 K matrix to describe the analytical part of the inverse amplitudes,

$$T^{-1}(s) = K^{-1}(s) - C(s). \tag{1}$$

The matrix elements $C_i(s)$ of the diagonal 2×2 Chew-Mandelstam (CM) function [32–34] $C(s) = C_i(s)\delta_{i,j}$ contain the right-hand cuts starting at the thresholds $s_{\mathrm{th},i} = (M_i + m_i)^2$. Here the masses are $M_1 = M_{D^0} + m_{\pi^+}$, $m_1 = M_{D^0}$, and $M_2 = M_{D^{*+}}$, $m_2 = M_{D^0}$ for the $D^0D^0\pi^+$ and D^0D^{*+} channels, respectively. Note that the $D^0\pi^+$ system is treated as an isobar of spin-1, and therefore, the T describes S-wave amplitudes. The CM function

$$C_i(s) = \frac{s}{\pi}\int_{s_{\mathrm{th}_i}}^{\infty} ds' \frac{\rho_i(s')}{s'(s'-s)} \tag{2}$$

is defined by the (quasi)two-body S-wave phase space factor $ImC_i(s) = \rho_i(s) = \lambda^{1/2}(s, M_i^2, m_i^2)/s$, explicitly,

$$\begin{aligned} &C_i(s; M_i, m_i) \\ &= \left[\frac{M_i^2 - m_i^2}{\pi s} - \frac{M_i^2 + m_i^2}{\pi(M_i^2 - m_i^2)}\right]\ln\left(\frac{m_i}{M_i}\right) \\ &\quad + \frac{1}{\pi} + \frac{\rho_i(s)}{\pi}\ln\left[\frac{\sqrt{s_{\mathrm{th}_i} - s} - \sqrt{(M_i - m_i)^2 - s}}{\sqrt{s_{\mathrm{th}_i} - s} + \sqrt{(M_i - m_i)^2 - s}}\right]. \end{aligned} \tag{3}$$

With the threshold singularities accounted for by $C(s)$, the K matrix is analytical in the vicinity at thresholds, and in the effective range approximation it as approximated by a matrix of constants.

In the notation of [35,36] the s dependence of production amplitude for the processes $pp \to D^0D^0\pi^+ + X$ and $pp \to D^0D^{*+} + X$ can be represented by a two-dimensional vector

$$F_i(s) = \sum_{k=1}^{2} \alpha_k(s) T_{ki}(s), \tag{4}$$

where $\alpha_i(s)$ are regular functions of s on the physical cut. Since the range of invariant mass is small, with $\Delta\sqrt{s} \ll O(100\ \mathrm{MeV})$, we can safely ignore any variation in s of the production amplitudes $\alpha_i(s)$ and also approximate them by constants. Finally, the measured yield is proportional to the differential cross section and given by

$$\frac{dY_1}{d\sqrt{s}} = N p_1 |F_1|^2. \tag{5}$$

Here, $p_1 = \lambda(s, M_1^2, m_1^2)/2\sqrt{s}$ is the magnitude of the momentum of the π^+ in the center-of-mass frame. Since the overall number of events is fitted, we can absorb α_1 into the normalization factor N and thus we set $\alpha_1 = 1$.

III. FIT RESULTS AND DISCUSSION

We fit the amplitudes to the $D^0D^0\pi^+$ invariant mass spectrum [17,18] using MINUIT [37]. One needs to consider the resolution for the $D^0D^0\pi^+$ mass. Here we follow the experiment [18] and convolute Eq. (6) with the resolution function. For a data point with mass E_i, we get the yields for the bin

$$\begin{aligned} \frac{\mathrm{Yields}}{\Delta \mathrm{E}} = &\int_{(E_i-\Delta E/2)^2}^{(E_i+\Delta E/2)^2} ds \frac{N p_1 |F_1|^2}{2\Delta E\sqrt{s}} \\ &\times \left\{\sum_{j=1}^{2} \beta_j \exp\left[-\frac{1}{2}\left(\frac{\sqrt{s} - E_i}{\sigma_j}\right)^2\right]\right\}, \end{aligned} \tag{6}$$

where ΔE is the bin width, $\beta_1 = 0.778$, $\beta_2 = 0.222$, $\sigma_1 = 1.05 \times 263$ keV, and $\sigma_2 = 2.413 \times \sigma_1$ [18]. We find a unique solution with desired physical properties. The parameters of the fit are given in Table I and correspond to $\chi^2_{\mathrm{d.o.f.}} = 0.92$. Notice that the error of the parameters from MINUIT is much smaller than that from bootstrap [38], which is done by varying the data with experimental uncertainty multiplying a normal distribution function. The comparison between the data and the model is shown in Fig. 1. As can be seen, our amplitudes fit the data rather well. To study the resonance, we also enlarge the plot of our solution around the T_{cc}^+, multiplying N_b instead of N_a in Eq. (5), as shown in the bottom graph in Fig. 1. Once the $D^0D^0\pi^+ - D^0D^{*+}$ amplitudes are determined on the real axis, they can be analytically continued to extract the information about the singularities located on the nearby

TABLE I. Parameters of the best fit, as explained in the text. The K-matrix elements and production parameters α_i are dimensionless. The first uncertainty of the parameters is given from MINUIT, and the second (up and down) uncertainty is from bootstrap within 2σ. N_a is the normalization factor for the data in the full range, while N_b is for the data in the region of T_{cc}^+. The correlation matrix is given in the Supplemental Material [40].

$K_{11} = -0.01204 \pm 0.00691^{+0.03280}_{-0.07039}$
$K_{12} = K_{21} = 0.5080 \pm 0.0025^{+0.0348}_{-0.0700}$
$K_{22} = 1.4447 \pm 0.0015^{+0.0235}_{-0.0477}$
$\alpha_2 = -0.3024 \pm 0.0016^{+0.0261}_{-0.0583}$
$N_a = 1434.0 \pm 129.8^{+662.0}_{-964.8}\ \mathrm{GeV}^{-2}$
$N_b = 516.0 \pm 49.3^{+225.6}_{-363.4}\ \mathrm{GeV}^{-2}$
$\chi^2_{\mathrm{d.o.f.}} = 0.92$

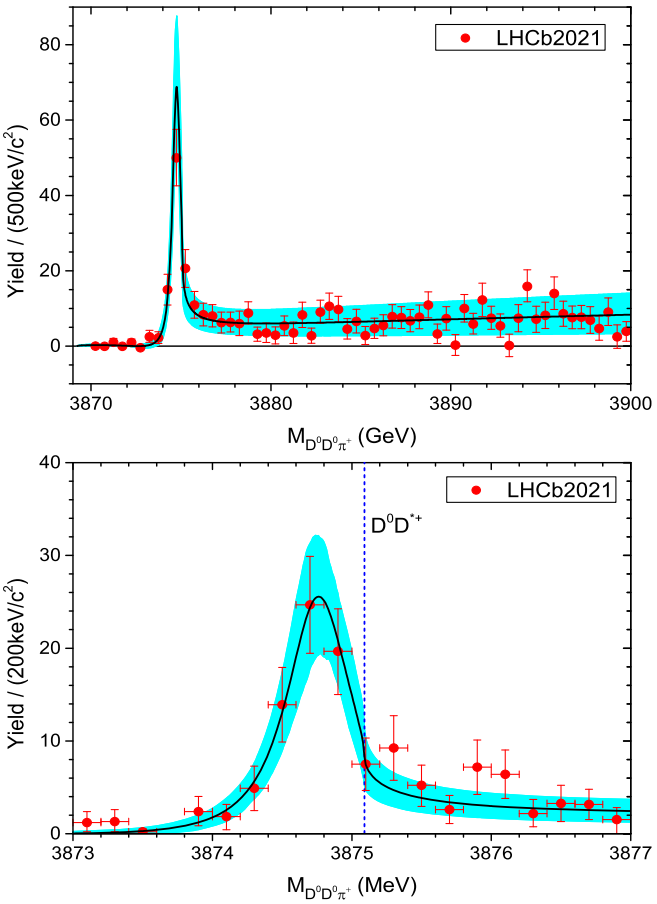

FIG. 1. The clear line shape from our solutions. The data points of $D^0D^0\pi^+$ invariant mass spectrum are superimposed. The cyan bands are taken from the bootstrap method within 2σ.

Riemann sheets (RSs). These are reached from the real s axis though the unitary cuts of the $C_i(s)$ functions. Near the pole, s_R residues/couplings in nth RS are computed from

$$T^n_{ij}(s) \simeq \frac{g^n_i g^n_j}{s^n_R - s}. \tag{7}$$

We find a single pole on RS-II, and the pole parameters are given in Table II. Here we follow the standard labeling of the sheets; e.g., the second sheet is reached from the physical region by moving into the lower complex plane between two thresholds [39]. The uncertainty of the pole parameters comes from the bootstrap within 2σ.

TABLE II. The pole location and its residues (both magnitude and phase) from our fit, in RS-II.

	$g^{II}_{D^0D^0\pi^+} = \lvert g\rvert e^{i\varphi}$		$g^{II}_{D^0D^{*+}} = \lvert g\rvert e^{i\varphi}$	
Pole location (MeV)	$\lvert g_1\rvert$ (GeV)	φ_1 (°)	$\lvert g_2\rvert$ (GeV)	φ_2 (°)
$3874.74^{+0.11}_{-0.04} - i0.30^{+0.05}_{-0.09}$	$0.22^{+0.03}_{-0.04}$	9^{+11}_{-5}	$0.69^{+0.04}_{-0.02}$	10^{+11}_{-5}

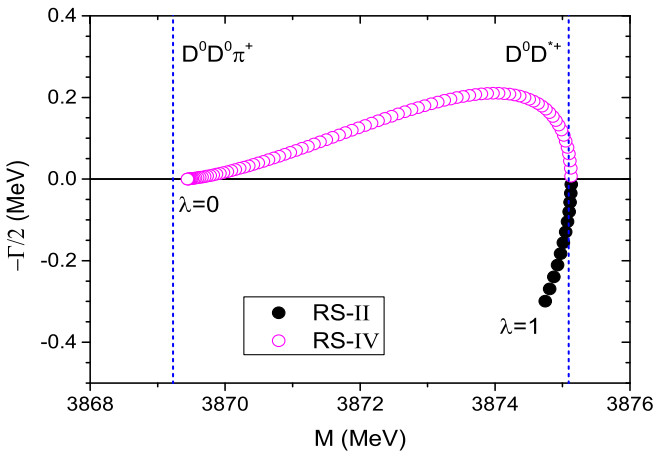

FIG. 2. The trajectories of pole locations by varying λ. The black filled circles are the poles in the second Riemann sheet $1 \geq \lambda \geq 0.88$, and the magenta open circles are the poles in the fourth Riemann sheet $0.87 \geq \lambda \geq 0$, respectively. The step of $\Delta\lambda$ is 0.01.

Notice that in the bootstrap method, where the data points are varied randomly, all the poles are located in RS-II. Since $|g_2| > |g_1|$, it appears that T^+_{cc} couples more strongly (roughly a factor of 3) to the D^0D^{*+} channel than to the $D^0D^0\pi^+$ channel. This supports the hypothesis that T^+_{cc} is a composite object dominated by the D^0D^{*+} component.

The trajectory of the pole on the second Riemann sheet is studied by varying λ which is introduced to modify the strength of coupling between the two channels $K_{12}(s) \to \lambda K_{12}(s)$, so that $\lambda = 1$ corresponds to the physical amplitude, while for $\lambda = 0$, Eq. (1) represents two uncoupled channels. As a function of λ, the pole trajectory is shown in Fig. 2. As λ decreases, the pole moves upward from the lower half $\sqrt{s}$ plane of RS-II to the upper half plane of RS-IV, crossing the real axis above the second (heavier) D^0D^{*+} threshold. This does not violate unitarity, since while moving from the second to the fourth sheet the pole never crosses the physical region. As this happens, the resonance bump seen on the real axis between thresholds moves toward the heavier threshold, and as the pole enters the fourth sheet it becomes a cusp. As λ is decreased further, the poles move below the lower threshold and into the real axis. Finally, it reaches the mass just ~0.21 MeV above the $D^0D^0\pi^+$ threshold. Notice that at the end of the trajectory with $\lambda = 0$ corresponding to the D^0D^{*+} single channel, the pole in the real axis below threshold is a virtual state. This implies that in the absence of channel coupling, the D^0D^{*+} system may not be sufficiently attractive to produce a molecule. If so, the T^+_{cc} is not a true bound state (a pole remaining on the second sheet) but an effect of a complicated interplay of weak attraction and channel interactions. This behavior is similar to that of the $P_c(4312)$, which was found to be likely an effect of weak interaction between $\Sigma^+_c\bar{D}^0$ and coupling the $J/\psi p$ channel [41].

To further assess systematic uncertainties, we include higher order terms in the effective range expansion. This slightly improves the fit quality but does not qualitatively change the amplitudes in the vicinity of the T_{cc}^{+}. In yet another check, we include the fit to the data without the resolution function. In this case, still only one pole is found in the RS-II $3874.75^{+0.12}_{-0.06} - i\,0.34^{+0.06}_{-0.12}$ MeV, with the residues of $|g_1| = 0.23^{+0.03}_{-0.04}$ GeV and $|g_2| = 0.70^{+0.03}_{-0.03}$ GeV. This is quite the same as what is found in Table II.

IV. ROLE OF THE D^* WIDTH

Since D^{*+} is unstable, its contribution to the spectral function corresponds to a branch cut (below the real axis) and not a pole. To account for that, we modify the Chew-Mandelstam C_2 accordingly [42]:

$$C_2(s) \to \frac{1}{\pi}\int_{s_{tr,D\pi}}^{\infty} ds' C(s;\sqrt{s'},m_2)\mathrm{Im}f_{D\pi}(s'), \qquad (8)$$

with $s_{\mathrm{th},D\pi} = (M_{D^0} + m_\pi^+)^2$ being the threshold for the reaction $D^0\pi^+ \to D^{*+} \to D^0\pi^+$ and $f_{D\pi}(s) = D^{-1}(s)$, the scattering amplitude in the single resonance approximation, with $D(s) = \tilde{M}^2 - s - \Sigma(s)$ and $\Sigma(s) = g^2(s - s_{\mathrm{th},D\pi})C(s;M_2,m_2)$ so that the imaginary part $\mathrm{Im}\Sigma(s) = g^2(s - s_{\mathrm{th},D\pi})\rho_2(s)$ is the energy-dependent width corresponding to the P-wave decay of the $D^{*+} \to D^0\pi^+$. With the parameters $g = 0.4451$ and $\tilde{M} = 2010.77$ MeV, the amplitude f reproduces the line shape of the D^* corresponding to a Breit-Wigner resonance with the pole at $M_{D^{*+}} - i\Gamma_{M_{D^{*+}}}/2 = 2010.26 - i\,0.04$ MeV. With this modification of $C_2(s)$, we fit the coupled channel amplitudes again, convoluting with Eq. (6) with the resolution function, and find a rather similar solution to the previous one. A pole is found in RS-II with $3874.76^{+0.08}_{-0.04} - i0.26^{+0.02}_{-0.09}$ MeV, and the residues are extracted as $|g_1| = 0.21^{+0.01}_{-0.04}$ GeV and $|g_2| = 0.71^{+0.02}_{-0.02}$ GeV. The pole trajectory is the same as what we found in Fig. 2, with only the pole moving toward but not reaching the real axis. Also, the destination of the pole (with $\lambda = 0$) is roughly 2.6 MeV above the $D^0D^0\pi^+$ threshold. These support the conclusion made before.

V. SUMMARY

In this paper, we performed an amplitude analysis on the invariant mass spectrum of $D^0D^0\pi^+$. The $D^0D^0\pi^+ - D^0D^{*+}$ coupled channel scattering amplitude is constructed using a K matrix within the Chew-Mandelstam formalism. Then we applied the Au-Morgan-Pennington method to study the final-state interactions for the invariant mass spectrum of $D^0D^0\pi^+$. A high-quality fit to the experiment data of LHCb [17,18] was obtained. We found a pole in the second Riemann sheet for the T_{cc}^{+}, with the pole location $3874.74^{+0.11}_{-0.04} - i0.30^{+0.05}_{-0.09}$ MeV. By reducing the strength of inelastic channels, we obtained the pole trajectory that suggests T_{cc}^{+} might be a D^0D^{*+} virtual state. Precise measurements of the line shape would be needed to further reduce theoretical uncertainties.

ACKNOWLEDGMENTS

We thank C. Fernández-Ramírez for helpful discussions on the bootstrap method. This work is supported by Joint Large Scale Scientific Facility Funds of the National Natural Science Foundation of China and the Chinese Academy of Sciences under Contract No. U1932110, the National Natural Science Foundation of China with Grants No. 11805059, No. 11805012, No. 11675051, and No. 12061141006, the Fundamental Research Funds for the central universities of China, and the U.S. Department of Energy Award No. DE-AC05-06OR23177 and No. DE-FG02-87ER40365.

[1] M. Gell-Mann, Phys. Lett. **8**, 214 (1964).
[2] G. Zweig, An SU(3) Model for Strong Interaction Symmetry and its Breaking, CERN Report No. 8182/TH.401.
[3] S. K. Choi *et al.* (Belle Collaboration), Phys. Rev. Lett. **91**, 262001 (2003).
[4] T. Aaltonen *et al.* (CDF Collaboration), Phys. Rev. Lett. **102**, 242002 (2009).
[5] A. Bondar *et al.* (Belle Collaboration), Phys. Rev. Lett. **108**, 122001 (2012).
[6] M. Ablikim *et al.* (BESIII Collaboration), Phys. Rev. Lett. **110**, 252001 (2013).
[7] Z. Q. Liu *et al.* (Belle Collaboration), Phys. Rev. Lett. **110**, 252002 (2013); **111**, 019901(E) (2013).
[8] M. Ablikim *et al.* (BESIII Collaboration), Phys. Rev. Lett. **111**, 242001 (2013).
[9] V. M. Abazov *et al.* (D0 Collaboration), Phys. Rev. D **89**, 012004 (2014).
[10] S. Chatrchyan *et al.* (CMS Collaboration), Phys. Lett. B **734**, 261 (2014).
[11] R. Aaij *et al.* (LHCb Collaboration), Phys. Rev. Lett. **118**, 022003 (2017).
[12] R. Aaij *et al.* (LHCb Collaboration), Phys. Rev. Lett. **125**, 242001 (2020).

[13] R. Aaij *et al.* (LHCb Collaboration), Phys. Rev. D **102**, 112003 (2020).
[14] F.-K. Guo, C. Hanhart, U.-G. Meißner, Q. Wang, Q. Zhao, and B.-S. Zou, Rev. Mod. Phys. **90**, 015004 (2018).
[15] Y.-R. Liu, H.-X. Chen, W. Chen, X. Liu, and S.-L. Zhu, Prog. Part. Nucl. Phys. **107**, 237 (2019).
[16] N. Brambilla, S. Eidelman, C. Hanhart, A. Nefediev, C.-P. Shen, C. E. Thomas, A. Vairo, and C.-Z. Yuan, Phys. Rep. **873**, 1 (2020).
[17] R. Aaij *et al.* (LHCb Collaboration), arXiv:2109.01038.
[18] R. Aaij *et al.* (LHCb Collaboration), arXiv:2109.01056.
[19] L. Y. Dai, M. Shi, G.-Y. Tang, and H. Q. Zheng, Phys. Rev. D **92**, 014020 (2015).
[20] X.-W. Kang, B. Kubis, C. Hanhart, and U.-G. Meißner, Phys. Rev. D **89**, 053015 (2014).
[21] L.-Y. Dai and M. R. Pennington, Phys. Rev. D **90**, 036004 (2014).
[22] I. V. Danilkin, C. Fernández-Ramírez, P. Guo, V. Mathieu, D. Schott, M. Shi, and A. P. Szczepaniak, Phys. Rev. D **91**, 094029 (2015).
[23] Y.-H. Chen, M. Cleven, J. T. Daub, F.-K. Guo, C. Hanhart, B. Kubis, U.-G. Meißner, and B.-S. Zou, Phys. Rev. D **95**, 034022 (2017).
[24] D.-L. Yao, L.-Y. Dai, H.-Q. Zheng, and Z.-Y. Zhou, Rep. Prog. Phys. **84**, 076201 (2021).
[25] S. S. Agaev, K. Azizi, and H. Sundu, Nucl. Phys. **B975**, 115650 (2022).
[26] A. Feijoo, W. H. Liang, and E. Oset, Phys. Rev. D **104**, 114015 (2021).
[27] Q. Qin, Y.-F. Shen, and F.-S. Yu, Chin. Phys. C **45**, 103106 (2021).
[28] N. Li, Z.-F. Sun, X. Liu, and S.-L. Zhu, Chin. Phys. Lett. **38**, 092001 (2021).
[29] X.-K. Dong, F.-K. Guo, and B.-S. Zou, Commun. Theor. Phys. **73**, 125201 (2021).
[30] X.-Z. Ling, M.-Z. Liu, L.-S. Geng, E. Wang, and J.-J. Xie, Phys. Lett. B **826**, 136897 (2022).
[31] P. A. Zyla *et al.* (Particle Data Group), Prog. Theor. Exp. Phys. **2020**, 083C01 (2020).
[32] G. F. Chew and S. Mandelstam, Phys. Rev. **119**, 467 (1960).
[33] B. J. Edwards and G. H. Thomas, Phys. Rev. D **22**, 2772 (1980).
[34] S.-Q. Kuang, L.-Y. Dai, X.-W. Kang, and D.-L. Yao, Eur. Phys. J. C **80**, 433 (2020).
[35] K. Au, D. Morgan, and M. Pennington, Phys. Rev. D **35**, 1633 (1987).
[36] L.-Y. Dai and M. R. Pennington, Phys. Lett. B **736**, 11 (2014).
[37] F. James and M. Roos, Comput. Phys. Commun. **10**, 343 (1975).
[38] B. Efron, Ann. Stat. **7**, 1 (1979).
[39] W. R. Frazer and A. W. Hendry, Phys. Rev. **134**, B1307 (1964).
[40] See Supplemental Material at http://link.aps.org/supplemental/10.1103/PhysRevD.105.L051507 for correlation matrix.
[41] C. Fernández-Ramírez, A. Pilloni, M. Albaladejo, A. Jackura, V. Mathieu, M. Mikhasenko, J. A. Silva-Castro, and A. P. Szczepaniak (JPAC Collaboration), Phys. Rev. Lett. **123**, 092001 (2019).
[42] J. L. Basdevant and E. L. Berger, Phys. Rev. D **19**, 239 (1979).